Human Molecular Genetics, 2011, Vol. 20, No. 3 **466–481**
doi:10.1093/hmg/ddq493
Advance Access published on November 11, 2010

Alström Syndrome protein ALMS1 localizes to basal bodies of cochlear hair cells and regulates cilium-dependent planar cell polarity

Daniel Jagger[1,*], Gayle Collin[2], John Kelly[1], Emily Towers[1], Graham Nevill[1], Chantal Longo-Guess[2], Jennifer Benson[3], Karin Halsey[3], David Dolan[3], Jan Marshall[2], Jürgen Naggert[2] and Andrew Forge[1]

[1]UCL Ear Institute, University College London, 332 Gray's Inn Road, London WC1X 8EE, UK, [2]The Jackson Laboratory, 600 Main Street, Bar Harbor, Maine 04609, USA and [3]Kresge Hearing Research Institute, University of Michigan, Ann Arbor, MI 48109, USA

Received September 10, 2010; Revised and Accepted November 7, 2010

Alström Syndrome is a life-threatening disease characterized primarily by numerous metabolic abnormalities, retinal degeneration, cardiomyopathy, kidney and liver disease, and sensorineural hearing loss. The cellular localization of the affected protein, ALMS1, has suggested roles in ciliary function and/or ciliogenesis. We have investigated the role of ALMS1 in the cochlea and the pathogenesis of hearing loss in Alström Syndrome. In neonatal rat organ of Corti, ALMS1 was localized to the basal bodies of hair cells and supporting cells. ALMS1 was also evident at the basal bodies of differentiating fibrocytes and marginal cells in the lateral wall. Centriolar ALMS1 expression was retained into maturity. In *Alms1*-disrupted mice, which recapitulate the neurosensory deficits of human Alström Syndrome, cochleae displayed several cyto-architectural defects including abnormalities in the shape and orientation of hair cell stereociliary bundles. Developing hair cells were ciliated, suggesting that ciliogenesis was largely normal. In adult mice, in addition to bundle abnormalities, there was an accelerated loss of outer hair cells and the progressive appearance of large lesions in stria vascularis. Although the mice progressively lost distortion product otoacoustic emissions, suggesting defects in outer hair cell amplification, their endocochlear potentials were normal, indicating the strial atrophy did not affect its function. These results identify previously unrecognized cochlear histopathologies associated with this ciliopathy that (i) implicate ALMS1 in planar cell polarity signaling and (ii) suggest that the loss of outer hair cells causes the majority of the hearing loss in Alström Syndrome.

INTRODUCTION

Alström Syndrome is a rare pleiotropic condition caused by mutations in the *ALMS1* gene (1,2). The syndrome is also characterized primarily by retinal degeneration (retinitis pigmentosa), renal, hepatic and pulmonary disease, cardiomyopathy, childhood truncal obesity, insulin resistance, type-2 diabetes mellitus and mild-to-moderate bilateral sensorineural hearing loss (3–8). The localization of the disease-associated protein (ALMS1; www.ncbi.nlm.nih.gov/omim) to the ciliary basal body suggests that it contributes to ciliogenesis and/or normal cilium function (9,10), or centriolar stability (11). However, specific cellular roles have yet to be described for ALMS1, which has restricted our understanding of the disease. Alström Syndrome is thought to share a common etiology with the phenotypically similar Bardet–Biedl Syndrome (BBS), which has been studied more widely. The numerous BBS proteins (BBS1–15; www.ncbi.nlm.nih.gov/omim) interact functionally with one another (12,13), and have implicated roles in planar cell polarity (PCP), Wnt signaling, Sonic Hedgehog signaling and regulation, and microtubule-based intraflagellar transport (14–19). To our knowledge, interactions between BBS proteins and ALMS1 have not been reported.

*To whom correspondence should be addressed at: UCL Ear Institute, University College London, 332 Gray's Inn Road, London WC1X 8EE, UK. Tel: +44 2076798930; Fax: +44 2076798990; Email: d.jagger@ucl.ac.uk

The molecular dissection of the related ciliopathies has resulted in a growing understanding of cilium function (20,21). Primary cilia are known to be key organelles during development and play central roles in tissue homeostasis. Progressive deficits in sensory functions, particularly in vision and hearing (22), are common to most human ciliopathies. In the developing cochlea, cilia are involved in processes that determine patterning and morphogenesis of sensory and non-sensory cells in the organ of Corti (23–26) and also in the formation of V- or W-shaped stereociliary bundles on the apical surface of sensory hair cells (13,23,27,28). The organization of the organ of Corti thus provides an excellent model for the study of cilium-dependent PCP signaling (24,26).

In this study, we have investigated the molecular basis of the hearing loss in Alström Syndrome to provide a more comprehensive description of the cellular effects of this poorly understood disease and to decipher the role of ALMS1. As deficits in auditory function can be ascribed to numerous cellular loci beyond the organ of Corti (29), we have examined the sub-cellular localization of ALMS1 throughout the rodent cochlea and have studied the effects of *Alms1* mutations on various mouse cochlear tissues. We found that ALMS1 localized to the ciliary basal body and/or centrioles in multiple tissues during development and in the functionally mature cochlea. *Alms1*-disrupted mice (30) displayed peculiarities in their stereociliary bundles and mis-positioning of their primary cilia. Older mice also suffered hearing impairment associated with an accelerated loss of outer hair cells. These results identify a role for ALMS1 in the regulation of cilium-dependent PCP and suggest widespread roles for ALMS1 in mature cochlear function and homeostasis. The previously unrecognized cochlear histopathologies seen here may contribute to hearing loss in patients with Alström Syndrome.

RESULTS

ALMS1 localizes to the ciliary basal body of developing cochlear cells

To determine the sub-cellular localization of the Alström Syndrome protein (ALMS1) in cochlear tissues, we used a specific N-terminal antibody raised in rabbits (9). An anti-acetylated tubulin antibody was used to stain cytoplasmic microtubules and ciliary axonemes (13). The cochleae of neonatal mice and rats are structurally immature at birth, and there is extensive postnatal tissue differentiation up to and beyond postnatal day 12, the time of hearing onset. The primary sensory and non-sensory tissues were distinguishable in vibratome sections of the P1 rat cochlea (Fig. 1A). Within the organ of Corti, hair cells and supporting cells were clearly delineated (Fig. 1B). Immunofluorescence experiments using these sections detected ALMS1 in basal bodies at the base of cilia located at the apical (lumenal) pole of hair cells (‘kinocilia’) and supporting cells, and in mesenchymal fibrocytes on the underside of the basilar membrane (Fig. 1C). Surface views of whole-mount preparations of the organ of Corti revealed the regularity of the distribution of the basal bodies (Fig. 1D). ALMS1 immunofluorescence could be distinguished in basal body centriolar pairs. The anti-ALMS1 antibody and an anti-γ-tubulin antibody (a centrosomal marker) labeled the same sub-cellular structures, confirming the basal body localization of ALMS1 (Fig. 1E). In the developing cochlear lateral wall, ALMS1 localized to basal bodies in marginal cells and in mesenchymal fibroblasts in the spiral ligament (Fig. 1F). These cells differentiate subsequently to form otic fibrocytes in the spiral ligament of the mature cochlea, and a subpopulation undergo a mesenchyme to epithelial transition (31) to form the basal cell layer of stria vascularis, the cochlear ion transporting epithelium (32). Together, these observations confirmed ALMS1 as a centrosomal protein and as a component of the cochlear ciliary basal body proteome.

The kinocilia of hair cells do not play a role in sound transduction within the mature organ of Corti. In rat and mouse cochlear hair cells, the kinocilium begins to regress at around P8, once the stereociliary bundle has formed (33). However, the centrioles (previously forming the ciliary basal bodies) are retained in mature hair cells after the kinocilium has been completely reabsorbed. Immunofluorescence experiments were carried out to see if ALMS1 was expressed at retained centrioles in mature cochlear tissues (Fig. 1G–J). In vibratome sections of the functionally and structurally mature rat cochlea, there was persistent expression of ALMS1 in centrioles of hair cells and supporting cells in the organ of Corti (Fig. 1G). In the mature cochlear lateral wall (Fig. 1H), there was centriolar labeling in fibrocytes and in the basal cell and intermediate cell layers of stria vascularis (Fig. 1I). The basal cell layer was clearly distinguishable in phalloidin-stained tissue, due to the high concentration of actin in these cells (34). There was no ALMS1 detectable in mature marginal cells. In cells that retain their primary cilia into functional maturity, such as Reissner’s membrane epithelial cells, ALMS1 was detected in the basal body and centrosome (Fig. 1J).

Ciliogenesis appears normal in neonatal *Alms1*$^{-/-}$ mice but hair cells display stereociliary bundle abnormalities

The hair cell kinocilium has been proposed to play a role in the organization of the stereociliary bundle during ontogenesis (25,26,28). Its emergence on the apical surface of the hair cell and subsequent migration may be essential for constructing the characteristic short-to-long ‘staircase’-like arrangement of individual stereocilia and the stereotyped V-shaped orientation of outer hair cell bundles. The influence of ALMS1 on these processes was investigated by examining the stereociliary bundles and kinocilia of neonatal *Alms1* disrupted (*Alms1*$^{-/-}$) mice (30). To examine the interrelationships between the kinocilia and stereociliary bundles, P2 organ of Corti whole-mount preparations were incubated with an anti-acetylated tubulin antibody (to label axonemes of cilia) and fluorescently tagged phalloidin (to label actin-containing stereocilia). In the apical turn of control mice, the stereociliary bundles formed a regular V-shaped arrangement and were all oriented in the same direction (Fig. 2A). Kinocilia were located at the vertex of the V-shaped bundle in all cells, and their relative positions defined the PCP axis of the sensory epithelium (26). In *Alms1*$^{-/-}$ mice, there were mis-shapen bundles (Fig. 2B), and kinocilia were often mis-localized relative to the bundle vertex. Some individual bundles were not

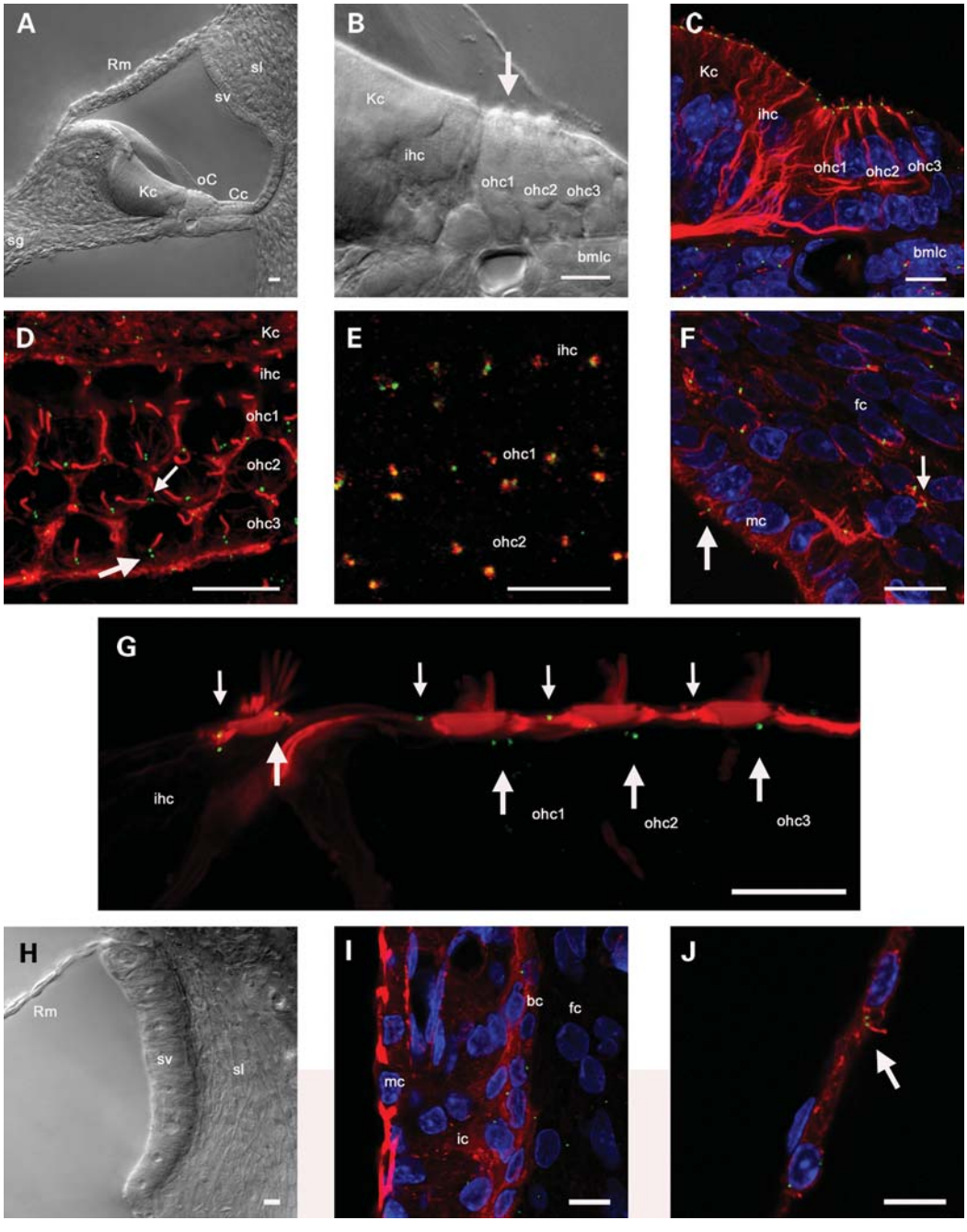

Figure 1. ALMS1 localizes to basal bodies in cochlear tissues. (**A** and **B**) DIC photo-micrographs of a cross-section of the basal turn region of a P1 rat cochlear slice. (A) The major tissue types are shown, including the organ of Corti (oC), Kölliker's cells (Kc), spiral ganglion (sg), stria vascularis (sv), spiral ligament (sl) and Reissner's membrane (Rm). (B) Detail of cells in the developing organ of Corti. Laterally, there are three rows of outer hair cells (ohc1–3), and medial to these are a single row of inner hair cells (ihc). Medial to the inner hair cells are Kölliker's cells (Kc), which are columnar epithelial supporting cells. Basilar membrane lining cells (bmlc) form a multi-cellular layer beneath the organ of Corti. The arrow depicts the direction of view for whole-mount preparations as in (**D**). (**C** and D) Projections of confocal image stacks of cochlear slices or whole-mount preparations labeled with antibodies against acetylated tubulin (red), which labels cytoplasmic microtubules and primary cilia, and ALMS1 (green). (C) Organ of Corti in a cochlear slice. ALMS1 localized to ciliary basal bodies at the apical poles of hair cells and supporting cells, and also in basilar membrane lining cells. (D) Surface view of a whole-mount preparation of the organ of Corti labeled with antibodies against acetylated tubulin and ALMS1. Basal body pairs showed a regular arrangement in hair cells (large arrow) and supporting cells (small arrow). (**E**) In a comparable surface view of a different whole-mount preparation, the ALMS1 immunofluorescence (green) was coincident with that of γ-tubulin (red), confirming the specificity of the ALMS1 antibody labeling to basal bodies. (**F**) Projection of a confocal stack through the lateral wall in a cochlear slice, labeled with antibodies against acetylated tubulin (red) and ALMS1 (green). The large arrow shows ALMS1 labeling of basal bodies in a marginal cell (mc) in stria vascularis, the small arrow shows ALMS1 labeling of basal bodies of a mesenchymal fibrocyte (fc) in spiral ligament. (**G**) Montage image showing details of the apices of apical turn hair cells in a P30 cochlear slice labeled with phalloidin (red) that labels filamentous actin in hair cell stereociliary bundles and apices of supporting cells and the antibody against ALMS1 (green). ALMS1 localized to centrioles in hair cells (large arrows) and supporting cells (small arrows). (**H**) DIC photo-micrograph of the cochlear lateral wall, showing Reissner's membrane (Rm), stria vascularis (sv) and spiral ligament (sl). (**I**) In the lateral wall, ALMS1 localized to centrioles of basal cells (bc), intermediate cells (ic) and fibrocytes (fc). Labeling was not apparent in marginal cells (mc). (**J**) ALMS1 (green) localized to basal bodies at the base of the primary cilium (acetylated tubulin, red) in a Reissner's membrane epithelial cell facing scala media. Scale bars, 10 μm.

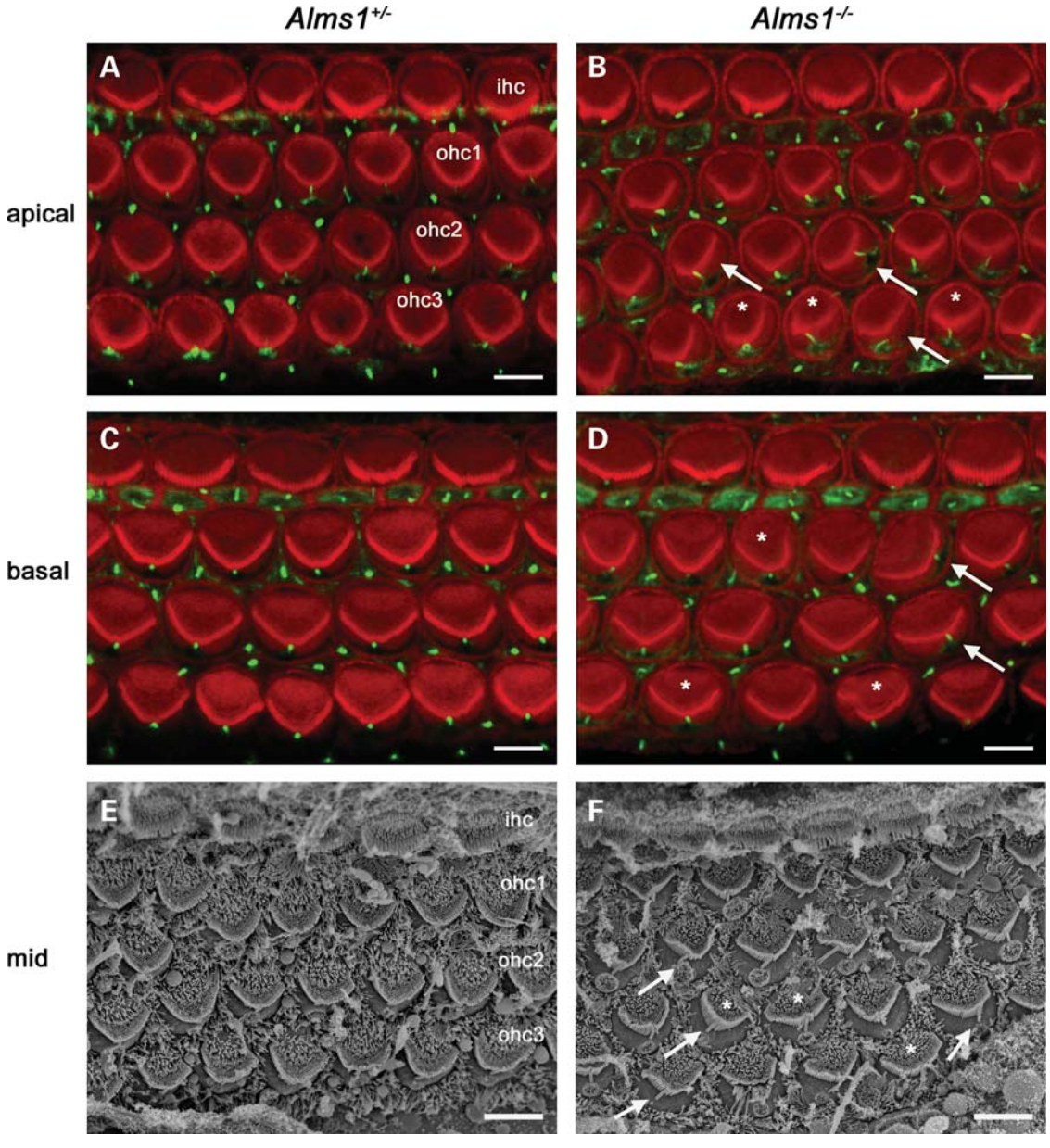

Figure 2. Planar polarity abnormalities in neonatal *Alms1*$^{-/-}$ mice hair cell stereociliary bundles. (**A**) Mid-apical turn organ of Corti whole-mount from a P2 *Alms1*$^{+/-}$ mouse stained with phalloidin (red) and an anti-acetylated tubulin antibody (green), demonstrating the regular arrangement of stereociliary bundles of inner hair cells (ihc) and outer hair cells (ohc1–3), and primary cilia of hair cells and supporting cells. The tubulin-rich kinocilia of outer hair cells were located at the vertex of the V-shaped bundles in all cells. (**B**) In the mid-apical turn of an *Alms1*$^{-/-}$ mouse organ of Corti some bundles were irregularly shaped (denoted *) and some were noticeably mis-oriented (arrows). Several kinocilia were not located at the vertex of the bundles. In mis-oriented bundles, the kinocilia were mis-localized relative to those in unaffected neighboring cells. (**C**) In the mid-basal turn organ of Corti of a P2 *Alms1*$^{+/-}$ mouse, the outer hair cell bundles were wider than in the apical turn (A), but were also regular in shape and the kinocilia were properly located at the bundle vertex. (**D**) In *Alms1*$^{-/-}$ mouse mid-basal turn organ of Corti, there were irregularly shaped bundles, mis-oriented bundles and mis-located kinocilia. (**E**) A scanning electron micrograph of a whole-mount of the mid-turn organ of Corti in a P2 *Alms1*$^{+/-}$ mouse demonstrated the regularity of the outer hair cell bundles. (**F**) In *Alms1*$^{-/-}$ mouse mid-turn organ of Corti, there were irregularly shaped and mis-oriented bundles (*) and mis-located kinocilia (arrows). Scale bars, 5 μm.

oriented correctly and the kinocilium of these cells appeared to be out of alignment with the PCP axis. In the basal turn of control mice (Fig. 2C), the outer hair cell bundles formed wider V-shapes than those in the apical turn, but the arrangement was comparably regular. The bundles in the basal turn of *Alms1*$^{-/-}$ mice were also mis-shapen and mis-oriented, and kinocilia were often mis-localized as seen in the apical turn (Fig. 2D). Scanning electron microscopy (SEM) further demonstrated the regularity of outer hair cell bundles in control animals (Fig. 2E) and the mis-localization of kinocilia relative to the bundle vertex in *Alms1*$^{-/-}$ mice (Fig. 2F). The bundles of inner hair cells in *Alms1*$^{-/-}$ mice appeared largely normal (Fig. 2B, D, F). This data suggested that in outer hair cells (but not in inner hair cells) of *Alms1*$^{-/-}$ mice, the initial

migration or subsequent anchoring of the kinocilium was abnormal. The N-terminal ALMS1 antibody labeled basal bodies of hair cells and supporting cells in both control mice and *Alms1*$^{-/-}$ mice (Supplementary Material, Fig. S1), consistent with the *Alms1* disruption in the gene-trap mice resulting in the absence of some but not all *Alms1* splice variants (30).

Mature *Alms1*$^{-/-}$ mice display hair bundle polarity defects but normal hearing function

In order to ascertain whether the hearing impairment in these mice can be related to hair cell defects, we studied the cyto-architecture in functionally mature *Alms1*$^{-/-}$ cochleae (Figs 3 and 4). Cochlear function reaches maturity around P21 in the mouse. SEM analysis of P22 control mice confirmed that outer hair cells were structurally mature (Fig. 3A and C), with characteristic 'V' or 'W' shaped stereociliary bundles depending on their tonotopic location. However, outer hair cell stereociliary bundles of P22 *Alms1*$^{-/-}$ mice displayed ultra-structural anomalies consistent with those seen in P2 cochleae (Fig. 3B and D). Some bundles were asymmetric (Fig. 3E), flattened (Fig. 3F) or mis-oriented (Fig. 3G), showing that the defects of the bundles occurring during development were retained into maturity. Although a small minority of hair bundles in control animals displayed very mild deformities (Fig. 3A), the extreme planar polarity deformities (asymmetry/flattening/mis-orientation) were never seen in control animals. To quantify the effect of *Alms1* disruption on hair bundle polarity, a series of $\times 1000$ magnification electron micrographs were taken of basal turn, mid-turn and apical turn regions of control and *Alms1*$^{-/-}$ littermates. The number of hair bundles that were noticeably deformed compared with their near neighbors were counted and calculated as a percentage of the total number of cells. In four control mice, there were 56 deformed bundles out of a total of 911 cells counted (6.1%), whereas in four *Alms1*$^{-/-}$ mice, there were 201/1158 (17.4%). In *Alms1*$^{-/-}$ mice, the proportion of affected bundles was independent of the tonotopic location (Fig. 4A). An analysis of the individual turns (Fig. 4B–D) showed no obvious trend between the proportion of deformed bundles and the cell row in which they were located. In two neonatal (P2) *Alms1*$^{-/-}$ mice, in which the bundle has yet to assume its mature arrangement, the occurrence of noticeably deformed bundles was comparable to that in P22 mice (140/605, 23.1%).

Outer hair cells contribute to normal hearing by acting as non-linear amplifiers. Consequently, in an additional group of animals, we tested auditory brainstem responses (ABRs) and distortion product otoacoustic emissions (DPOAEs), a measure of outer hair cell function. At low and mid frequencies (12 and 24 kHz), 1-month-old *Alms1*$^{-/-}$ mice had comparable ABRs with their littermate controls (Fig. 5A). At 48 kHz, two of the three *Alms1*$^{-/-}$ mice had slightly higher thresholds than controls. In a single *Alms1*$^{+/+}$ mouse (Fig. 5B), there were DPOAEs in response to 12 and 24 kHz tones at low sound intensities (<60 dB), but DPOAEs in response to 48 kHz tones were only recorded at higher sound intensities (>60 dB). These results are consistent with previous observations for wild-type mice (35). In a single *Alms1*$^{-/-}$ littermate (Fig. 5C), there were robust DPOAEs at low to mid frequencies, but not at 48 kHz. Group data for 12 kHz (Fig. 5D) and 24 kHz (Fig. 5E) showed that DPOAEs were largely indistinguishable between 1-month-old control and *Alms1*$^{-/-}$ mice.

Alms1$^{-/-}$ mice display progressive hair cell loss and decreased hearing sensitivity

Analysis of the organ of Corti of older animals revealed further progressive differences between *Alms1*$^{-/-}$ mice and their littermate controls (Fig. 6). There was loss of outer hair cells from the organ of Corti of control mice in a progressive apex to base pattern, but this loss was more extensive in the mid and basal turns of three 7-month-old *Alms1*$^{-/-}$ mice analyzed. In the apical turn of 7-month-old control mice, there was little loss of outer hair cells (Fig. 6A). In age-matched *Alms1*$^{-/-}$ mice, there was also little cell loss in the apical turn (Fig. 6B), although remaining cells showed typical bundle abnormalities. In the mid-turn region of control mice, there was scattered loss of outer hair cells (Fig. 6C), but in *Alms1*$^{-/-}$ mice the loss was greater (Fig. 6D). The upper basal turn of control mice showed scattered cell loss (Fig. 6E), but the equivalent region in *Alms1*$^{-/-}$ mice was almost devoid of outer hair cell bundles (Fig. 6F). The apex to base loss of outer hair cells in control animals was typical for the C57BL/6 background strain on which this model was raised, and which is recognized as a model of early onset hearing loss (36). Transmission electron microscopy (TEM) analysis of organ of Corti in similarly aged *Alms1*$^{-/-}$ mice (P191) showed that surviving outer hair cells in the apical turn appeared largely normal (Fig. 6G), as did their innervation (Fig. 6H). In the basal turn, the loss of outer hair cells was apparent (Fig. 6I), whereas inner hair cells survived. Following the loss of outer hair cells, the supporting cells had carried out a normal repair process, by migrating into the spaces left by the loss of hair cells (37).

In a separate group of 6–7-month-old animals, *Alms1*$^{-/-}$ mice had relatively higher ABR thresholds at low and mid frequencies (Fig. 7A), although thresholds were high for all animals at 48 kHz. A single 6-month-old *Alms1*$^{+/+}$ mouse (Fig. 7B) had DPOAEs in response to 12 and 24 kHz tones (>40 dB), but not in response to 48 kHz tones. A single *Alms1*$^{-/-}$ littermate (Fig. 7C) only had DPOAEs at 12 kHz at high sound levels (>60 dB) and did not respond to 24 kHz tones at any sound level. Group data for 12 (Fig. 7D) and 24 kHz (Fig. 7E) confirmed the lack of DPOAEs in *Alms1*$^{-/-}$ mice, suggesting that hearing losses in these older animals could be attributed, at least in part, to a loss of outer hair cell function.

Ultrastructural defects in stria vascularis of *Alms1*$^{-/-}$ mice

Immunofluorescence experiments in the developing and mature cochlea revealed an almost ubiquitous expression pattern of ALMS1, suggesting this ciliary protein may play a role in cochlear tissues beyond the organ of Corti. Consequently, we have carried out a comparison of other cochlear tissues in control and *Alms1*$^{-/-}$ mice (Fig. 8), in particular

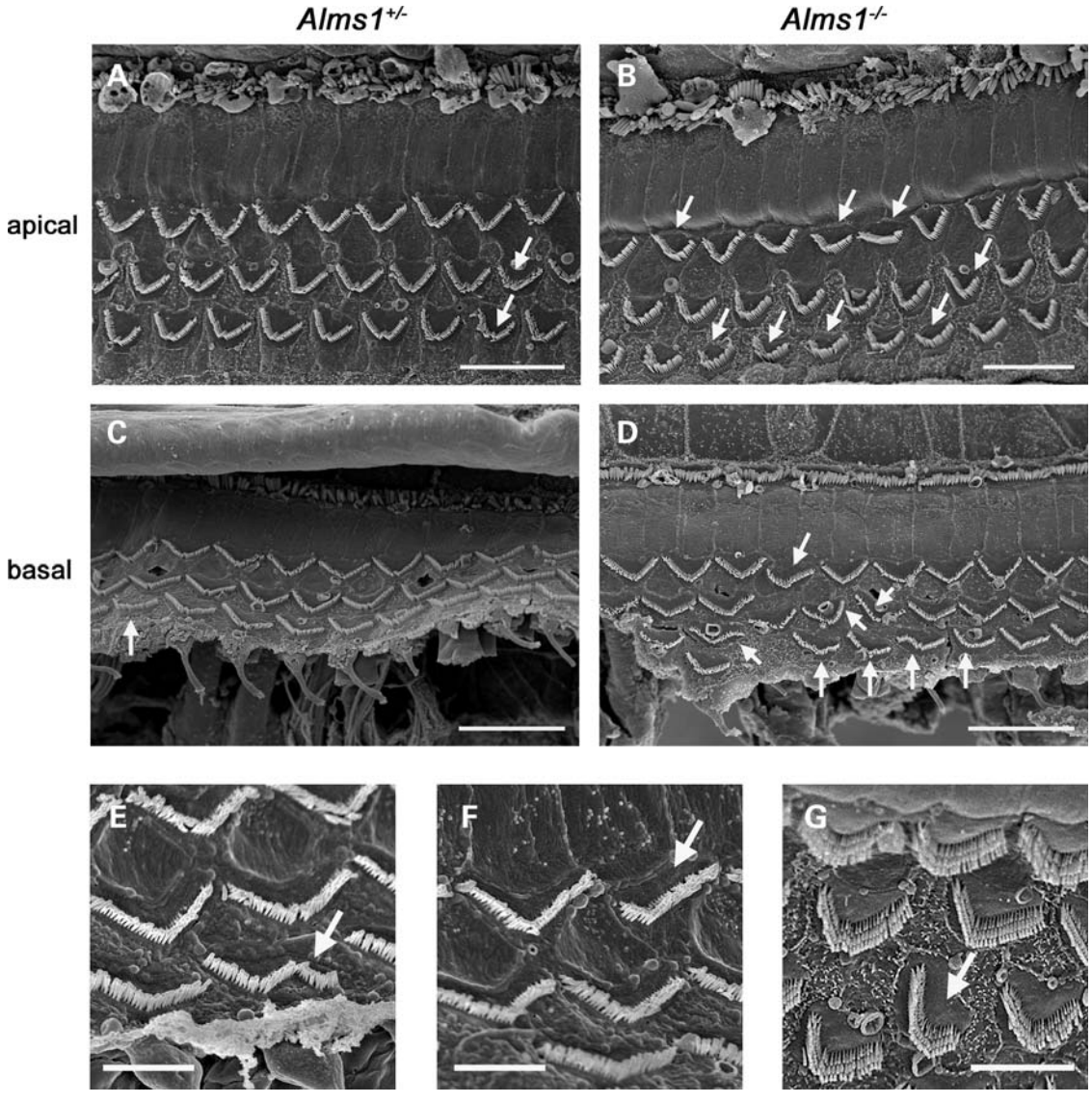

Figure 3. Planar polarity abnormalities of hair cell stereociliary bundles in juvenile *Alms1*$^{-/-}$ mice. (**A**) Scanning electron micrograph of an apical turn organ of Corti whole-mount from a P22 *Alms1*$^{+/-}$ mouse. Outer hair cell stereociliary bundles were arranged in a regular pattern, although occasional mis-shapen bundles could be identified (arrows). (**B**) In the P22 *Alms1*$^{-/-}$ mouse organ of Corti, there were various examples of mis-shapen bundles in all three rows of outer hair cells (arrows). (**C**) Basal turn organ of Corti whole-mount from a P22 *Alms1*$^{+/-}$ mouse. (**D**) Basal turn organ of Corti whole-mount from a P22 *Alms1*$^{-/-}$ mouse, showing various bundle abnormalities (arrows). (**E**–**G**) Detail of outer hair cells with asymmetric (**E**), flattened/asymmetric (**F**) and mis-oriented/asymmetric (**G**) bundles. Scale bars: (A–D) 20 μm, (E–G) 5 μm.

the cochlear lateral wall (Fig. 8A and D). Whereas the stria vascularis of control mice was normal in appearance (Fig. 8B and E), there were large spaces in the stria vascularis of *Alms1*$^{-/-}$ mice (Fig. 8C and F). These spaces appeared most noticeably in the intermediate cell layer, with the basal cell and marginal cell layers remaining largely intact. Similar spaces were observed, although to a lesser degree, in the stria vascularis of P24 *Alms1*$^{-/-}$ mice (Supplementary Material, Fig. S2). The apical (lumenal) membrane of marginal cells in 6-month-old *Alms1*$^{-/-}$ mice showed an unusual feature, with large blebs extending into scala media (Fig. 8F). The large spaces in stria vascularis could also be demonstrated in cryosections immunolabeled with an antibody against acetylated tubulin (detecting microtubules in marginal cells) and counterstained with phalloidin (to label the actin-rich basal cells; Fig. 8G–H). The spaces appeared in all turns of the cochlea (Fig. 8G), and some very large lesions were evident (Fig. 8H). The defects in the cellular integrity suggested that the function of stria vascularis in *Alms1*$^{-/-}$ mice might have been compromised. However, the endocochlear potential (EP) in two 6-month-old *Alms1*$^{-/-}$ mice were within the normal range ($>+80$ mV; Fig. 8I).

The spaces that appeared in stria vascularis of *Alms1*$^{-/-}$ mice were further investigated using TEM (Fig. 9). In 80 nm sections from 6-month-old control mice, all the major subtypes of cells in stria vascularis were observed (Fig. 9A). Marginal cells had characteristic eliptoid nuclei and numerous basolateral projections extending into the intermediate cell

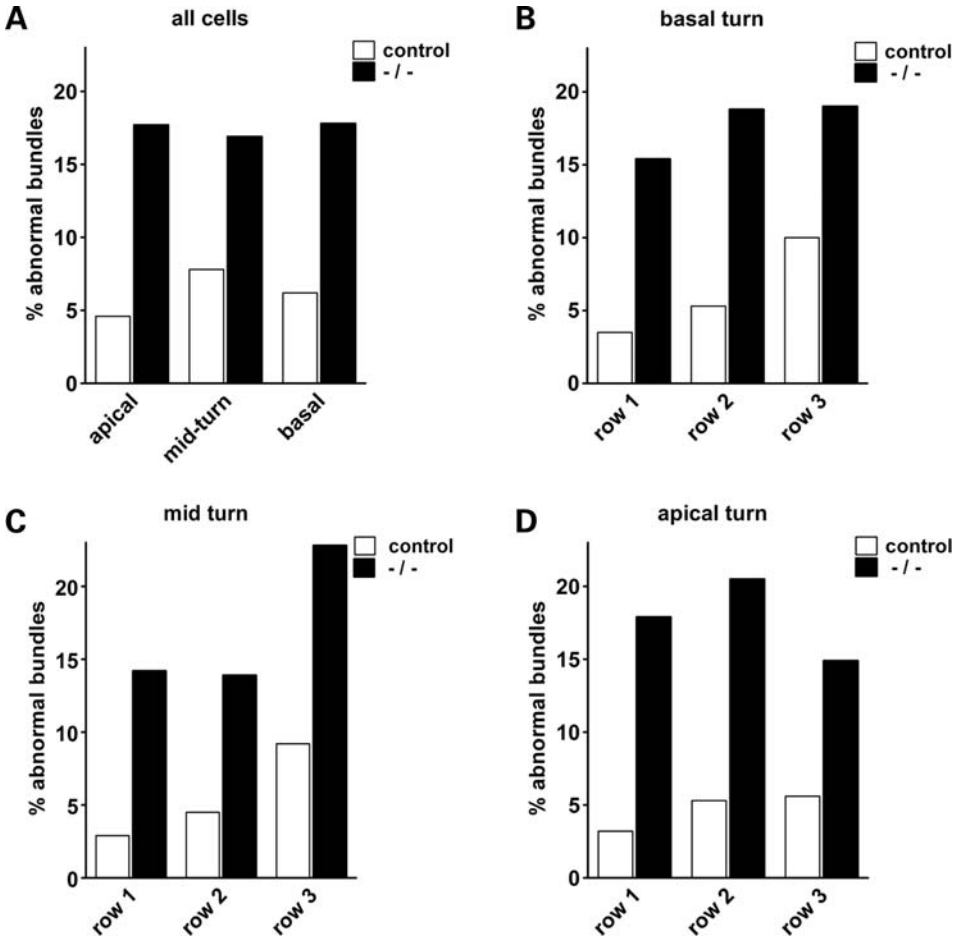

Figure 4. Proportion of outer hair cell stereociliary bundles displaying planar polarity abnormalities in juvenile control and *Alms1*$^{-/-}$ mice. (**A**) Number of noticeably abnormal outer hair cell bundles as a proportion of total cells, within the apical, mid-turn and basal regions of the cochlea. (**B**) Counts for the basal turn region, within the innermost cell row (row 1), middle row (row 2) and outermost row (row 3). (**C**) Counts for the mid-turn region. (**D**) Counts for the apical turn region.

layer (Fig. 9B). Vasculature appeared normal (Fig. 9C), with an intact basement membrane surrounding the blood vessel. In *Alms1*$^{-/-}$ mice, the large spaces were evident throughout the stria vascularis (Fig. 9D). Close examination of marginal cells revealed that they had unusually shaped nuclei. Some had intracellular vacuoles (Fig. 9E) and blebs extending from the apical membrane (Fig. 9E–F). At the marginal cell apex beneath the blebs, there were circumferential microfilament assemblies (Fig. 9F). These assemblies were not observed in marginal cells in control mice (Fig. 9B). In the intermediate cell layer of *Alms1*$^{-/-}$ mice, there were intracellular membrane-bound vacuoles (Fig. 9G), some of which deformed the cell nucleus (Fig. 9H), indicating they were located within the cell. Vasculature appeared normal in *Alms1*$^{-/-}$ mice (Fig. 9I), suggesting that the histopathology was not caused by defects in blood vessel integrity or permeability. The histopathology seen in *Alms1*$^{-/-}$ mice was most likely not a fixation artifact, as other cochlear tissues appeared normal, and in stria vascularis sub-cellular organelles (e.g. mitochondria, Fig. 9F) had a normal appearance. Also, the histopathology was seen in *Alms1*$^{-/-}$ mice from several litters tested, but never in control mice. The vacuoles within stria vascularis cells were not seen in surviving outer hair cells within the same TEM sections (Fig. 6G–H). The defects in stria vascularis of *Alms1*$^{-/-}$ mice were not seen in age-matched *Bbs6*$^{-/-}$ mice or *Bbs4*$^{-/-}$ mice (Supplementary Material, Fig. S3), which were raised on the same background strain (23). This suggests that the observed defects were caused by *Alms1* disruption and unrelated to the background strain.

To investigate the effects of the stria vascularis abnormalities further, cochlear cryosections of control and *Alms1*$^{-/-}$ mice were immunolabeled with primary antibodies raised against cell-specific proteins (Supplementary Material, Figs. S2 and S4). We used an antibody against KIR4.1, an inwardly rectifying potassium channel expressed by intermediate cells (38). In control mice, KIR4.1 immunofluorescence clearly delineated the intermediate cells, which lay in a continuous layer between the basal cell layer and the marginal cell layer (Supplementary Material, Figs S2C–D and S4A). Intermediate cells had a characteristic morphology, with multiple dendrite-like projections that extended apically from the cell body, and wrapped around blood vessels just below the level of marginal cell nuclei. In older *Alms1*$^{-/-}$ mice, there were

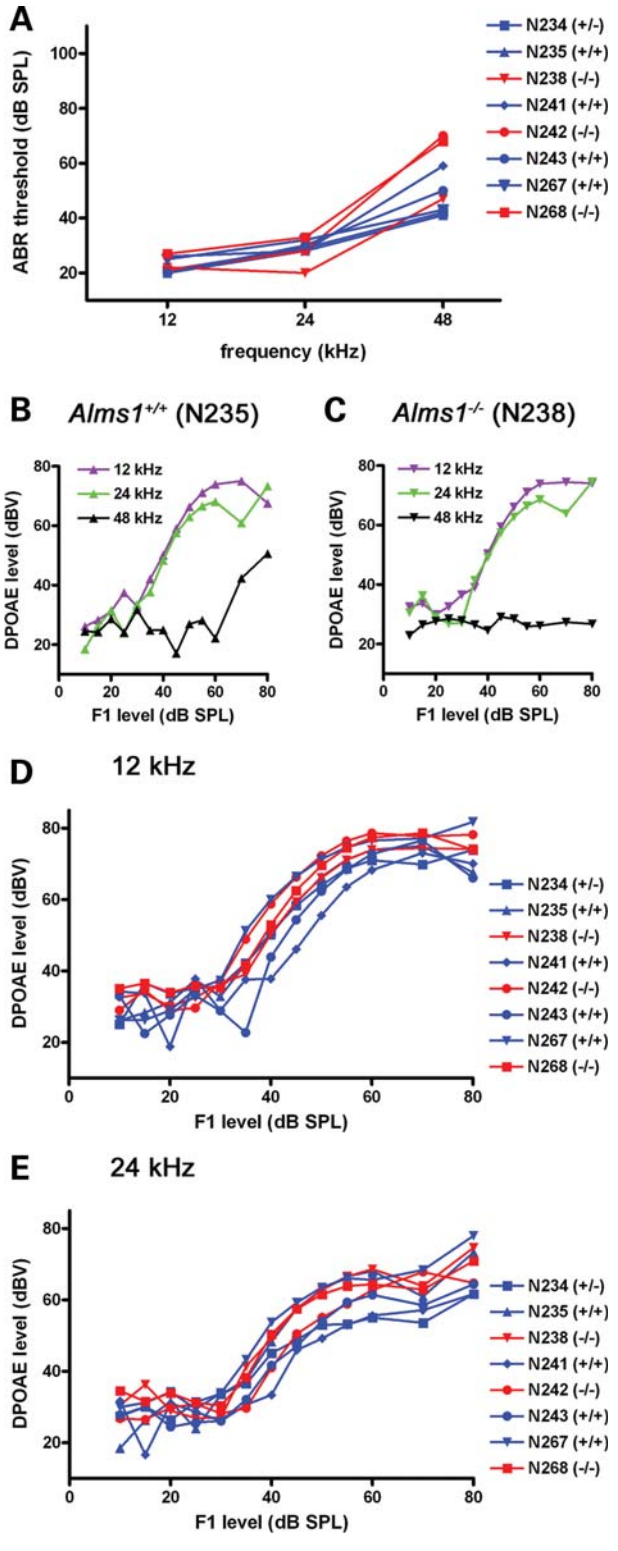

Figure 5. Outer hair cell function in juvenile *Alms1*$^{-/-}$ mice was normal. (**A**) ABR thresholds of 1-month-old *Alms1*$^{-/-}$ mice (red) were comparable with those of control animals (blue). (**B** and **C**) Comparable DPOAEs in a single control mouse (B) and an *Alms1*$^{-/-}$ littermate (C) in response to low (12 kHz) and mid (24 kHz) frequency tones. DPOAEs were not activated in the *Alms1*$^{-/-}$ mouse at 48 kHz, and were only activated at sound levels >60 dB in the control mouse. (**D**–**E**) Group data showed the similarities between DPOAEs in both sets of mice at 12 kHz (**D**) and 24 kHz (**E**).

regions within stria vascularis where KIR4.1-labeled cells were comparable with controls, but there were also regions that were devoid of KIR4.1 immunofluorescence (Supplementary Material, Fig. S4A–B). As KIR4.1-labeled intermediate cells were fully present in P24 *Alms1*$^{-/-}$ mice (Supplementary Material, Fig. S2), these data suggest that there was a progressive loss of intermediate cells even though surviving cells had normal KIR4.1 expression levels. In tissue labeled with an antibody against GLUT1, a glucose transporter expressed in basal cells and vascular pericytes (34), there were no obvious differences between control (Supplementary Material, Fig. S4C) and *Alms1*$^{-/-}$ mice (Supplementary Material, Fig. S4D). An antibody raised against KCNQ1, a potassium channel expressed in the apical membrane of marginal cells (32), labeled marginal cells in both control (Supplementary Material, Fig. S4E) and *Alms1*$^{-/-}$ mice (Supplementary Material, Fig. S4F), suggesting normal expression in these cells. However, KCNQ1-labeled marginal cells were absent from discrete regions of stria vascularis in *Alms1*$^{-/-}$ mice. An antibody raised against connexin30 (CX30), a gap junction channel subunit expressed widely throughout the cochlea (39), labeled intercellular junctions between otic fibrocytes, basal cells and intermediate cells in both mutant and control mice (Supplementary Material, Fig. S4G–H). This suggests that gap junction formation is unaffected in *Alms1*$^{-/-}$ mice.

Together, these data suggest that in addition to the hair cell peculiarities responsible for decreased hearing sensitivity, there is also a progressive degeneration of the stria vascularis in *Alms1*$^{-/-}$ mice. In animals that showed significant hearing loss, EP was normal and proteins necessary for the generation of EP were expressed at normal levels at all ages studied. The lateral wall histopathology occurred initially as intracellular vacuoles within intermediate cells and subsequently within marginal cells. In some older mice large lesions were evident, caused by the apparent loss of intermediate cells and also marginal cells.

DISCUSSION

We have identified previously unrecognized cochlear histopathologies in the organ of Corti and stria vascularis in a mouse model for human Alström Syndrome. *Alms1*-disrupted (*Alms1*$^{-/-}$) mice displayed hair cell stereociliary bundle abnormalities typical of PCP defects. Although juvenile *Alms1*$^{-/-}$ mice showed normal hearing sensitivity, older *Alms1*$^{-/-}$ mice showed hearing losses at all frequencies compared with their age-matched littermates. The hearing loss can be explained by an age-dependent degeneration of outer hair cells. The atrophy of stria vascularis, associated with a loss of intermediate cells, probably did not contribute to the hearing loss in animals of the ages studied, as EP was measured within the normal range. Both these pathologies appeared typical of defective tissue homeostasis, resulting from the loss of the disease-associated protein ALMS1.

Alström Syndrome is a human ciliopathy characterized by progressive sensory dysfunction

Alström Syndrome is an autosomal recessive condition in which patients suffer from a complex array of pathologies

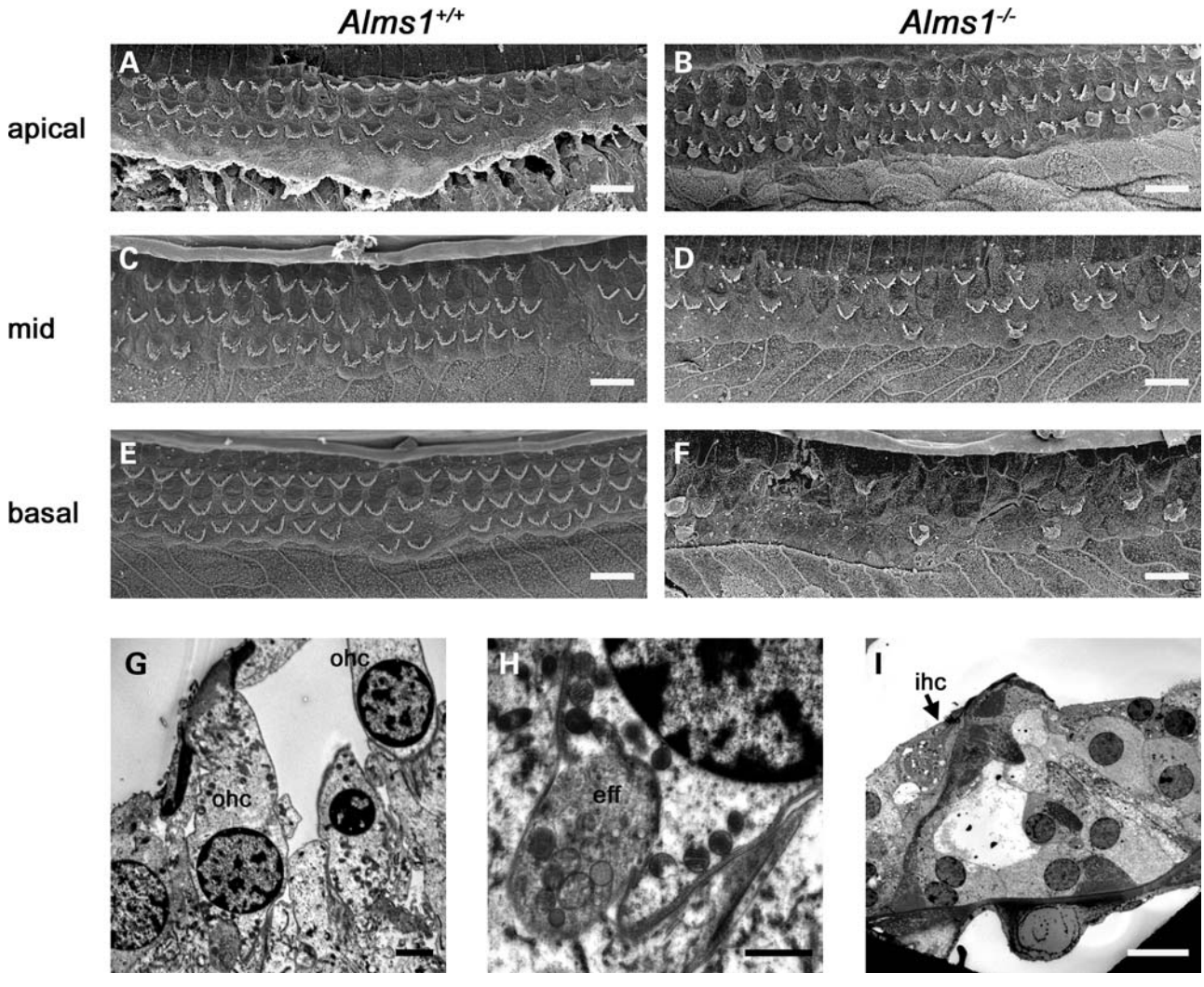

Figure 6. Outer hair cell loss in older control and *Alms1*$^{-/-}$ mice. (**A**)–(**F**) show scanning electron micrographs of organ of Corti whole-mount preparations from P213 *Alms1*$^{+/+}$ (A, C, E) and *Alms1*$^{-/-}$ (B, D, F) mice. (A) In the apical turn of the *Alms1*$^{+/+}$ mouse cochlea, there were few outer hair cells missing. (B) In the apical turn of the *Alms1*$^{-/-}$ mouse cochlea, there were few missing cells but surviving cells displayed bundle abnormalities. (C) In the mid-turn region of the *Alms1*$^{+/+}$ mouse, there was scattered cell loss. (D) In the mid-turn region of the *Alms1*$^{-/-}$ mouse, the cell loss was more extensive. (E) In the upper basal region of the *Alms1*$^{+/+}$ mouse, there was scattered cell loss. (F) In the basal turn of the *Alms1*$^{-/-}$ mouse, the cell loss was extensive, with only few outer hair cells remaining. (**G**)–(**I**) show transmission electron micrographs of organ of Corti from P191 *Alms1*$^{-/-}$ mice. (G) Surviving outer hair cells (ohc) in the apical turn. (H) Detail of the sub-nuclear synaptic region of a surviving outer hair cell. An efferent nerve ending (eff) attached to the outer hair cell appeared normal. (I) In the basal turn, outer hair cells had been lost, but an inner hair cell (ihc) survived. Supporting cells migrated to fill the spaces arising from outer hair cell loss. Scale bars: (A–F, I) 10 μm, (G) 2 μm, (H) 1 μm.

(3–6). ALMS1 is a 461 kDa protein consisting of 4169 amino acids (1,2). The C-terminus of ALMS1 contains an 'ALMS motif' of 120 amino acid residues which share sequence similarity with centriolar proteins, C10orf90 and KIAA1731 (1,11). While sequence analysis has revealed potential nuclear localization signals (amino acids 3805–3830 and amino acids 3937–3954), a leucine zipper motif (amino acids 2480–2501) and a serine-rich region (amino acids 3857–3873), the functional significance of these regions has not yet been thoroughly studied. The life-threatening aspects of the disease have been attributed tentatively to the abnormal function of primary cilia (9) or to effects on ciliogenesis and cilium survival (10). Common to all patients are progressive losses of vision and hearing, which commence during early childhood. Retinal cone-rod dystrophy is initially evidenced by nystagmus and photophobia in infants (5). By 16 years of age, approximately 90% of patients are completely blind. Histopathological observations in post-mortem adult retinal tissue show abnormalities in all retinal layers, optic nerve atrophy, attenuated vessels and nearly total absence of photoreceptors (4). Retinal immunohistochemical studies in *Alms1*$^{-/-}$ mice demonstrate mis-localization of rhodopsin to the outer nuclear layer (30). Bilateral sensorineural hearing loss appears during childhood (mean onset age approximately 5 years) and is compounded by frequent incidences of chronic otitis media and glue ear (4,7). Most patients are reliant on the use of bilateral hearing aids for normal communication, and with the total loss of vision it is essential to maximize and protect their residual hearing.

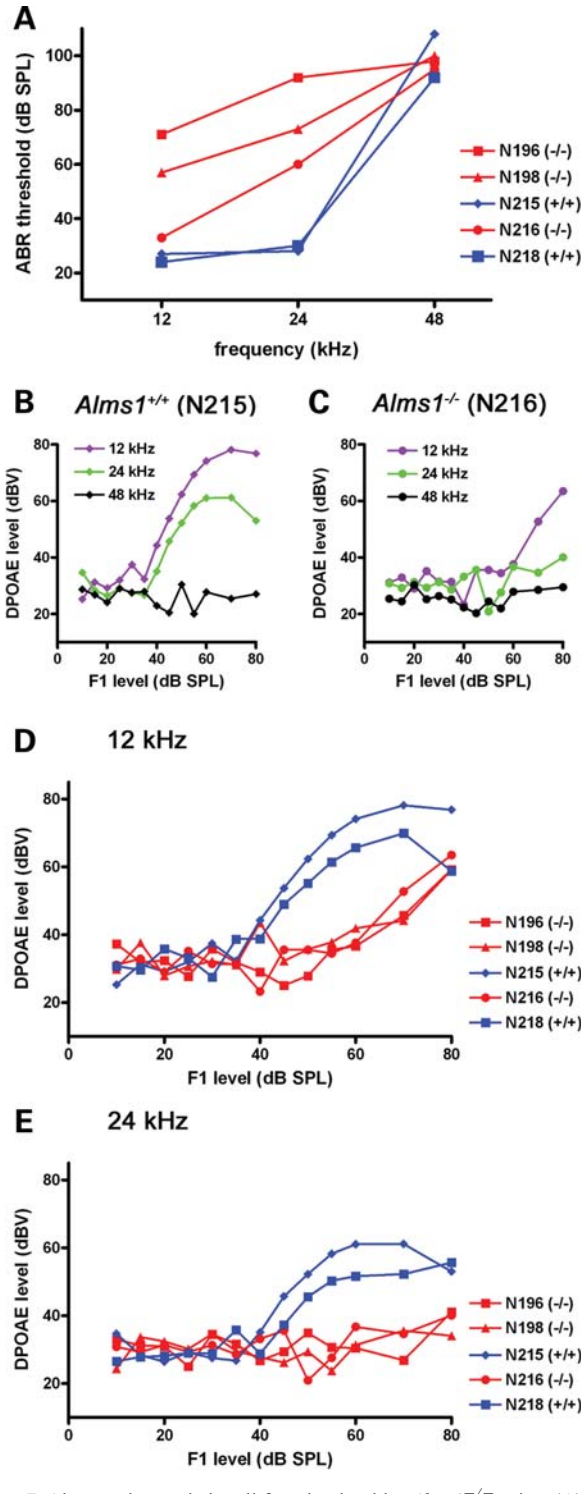

Figure 7. Abnormal outer hair cell function in older *Alms1*$^{-/-}$ mice. (**A**) ABR thresholds of 6–7-month-old *Alms1*$^{-/-}$ mice (red) were higher than those of control animals (blue) at low (12 kHz) and mid (24 kHz) frequencies. Thresholds were high in all animals at 48 kHz. (**B**) In a single control mouse, DPOAEs were recorded in response to low and mid frequency tones (>35 dB), but not at 48 kHz. (**C**) In an *Alms1*$^{-/-}$ littermate, DPOAEs were impaired at all frequencies. (**D** and **E**) Group data reflected the differences between DPOAEs in the control (blue) and *Alms1*$^{-/-}$ (red) mice at 12 kHz (D) and 24 kHz (E).

Audiometric data from Alström Syndrome patients reveal a comparable loss of hearing sensitivity across all frequencies, which often result in a characteristic 'flat' audiogram (7). In addition to the loss of outer hair cell function, the flat audiogram may be diagnostic of strial dysfunction (40), as caused by diuretic inhibition of strial ion transport mechanisms (41), or in atrophic strial presbyacusis (42). The possibility of strial dysfunction in human Alström Syndrome is supported by our observation of strial atrophy in *Alms1*$^{-/-}$ mice. Despite this advancing strial atrophy, EP was recorded within the normal range suggesting that this pathology did not contribute to the hearing loss in these animals at 6–7 months of age. This result may not be surprising though. Stria vascularis can degenerate by as much as 70%, to what visibly appears to be a non-functional state, with only around a 25 mV decline in EP (43). This points to a degree of redundancy in strial ion transport capacity and suggests that stria vascularis has to degenerate further in *Alms1*$^{-/-}$ mice, to a critical point before EP declines to non-functional levels. The strial histopathology in *Alms1*$^{-/-}$ mice appears distinct to that seen in mouse models of Pendred syndrome (44) or hypothyroidism (45), which also suffer dysfunction of stria vascularis. In these models, intermediate cells are present, but KIR4.1 (KCNJ10) channel expression is impaired. In 3-week-old *Alms1*$^{-/-}$ mice, KIR4.1 was normally distributed prior to the loss of intermediate cells. In noise-exposed mice, there are histopathological effects that are similar to those we have observed in *Alms1*$^{-/-}$ mice (46). Large intracellular vacuoles appear in fibrocytes of noise-exposed mice, and there is subsequent chronic loss of fibrocytes, swelling of marginal cells and disintegration of intermediate cells. It may be of relevance to the care of Alström Syndrome patients to examine the noise-sensitivity of *Alms1*$^{-/-}$ mice.

Hearing loss in *Alms1*$^{-/-}$ mice results from dysfunctional amplification

We have observed peculiarities in outer hair cells in *Alms1*$^{-/-}$ mice that were present at birth and persisted with a comparable occurrence into adulthood. These included malformation and mis-orientation of stereociliary bundles, which occurred with approximately equal regularity between rows, and along the length of the cochlear partition. In young adult mice (around 1 month old), DPOAEs appeared normal, suggesting that the ensemble contribution of outer hair cells to the cochlear amplifier was largely unaffected. As such, it would appear that the *Alms1*-dependent structural defects are not directly responsible for the hearing loss in these animals. In older *Alms1*$^{-/-}$ mice, DPOAEs were absent at higher frequencies, and even were poor at lower frequencies, which was predicted from the extensive loss of outer hair cells compared with control animals. Control animals suffered some loss of outer hair cells from the basal turn, and consequently had poorer DPOAEs and more hearing loss at high frequencies. These losses were not beyond those expected for animals raised on the C57BL/6J background strain, which is recognized widely as a model of age-related hearing loss (36). *Alms1*$^{-/-}$ mice suffered from an accelerated loss of outer hair cells that were most prevalent at basal locations. It seems unlikely, therefore, that outer hair

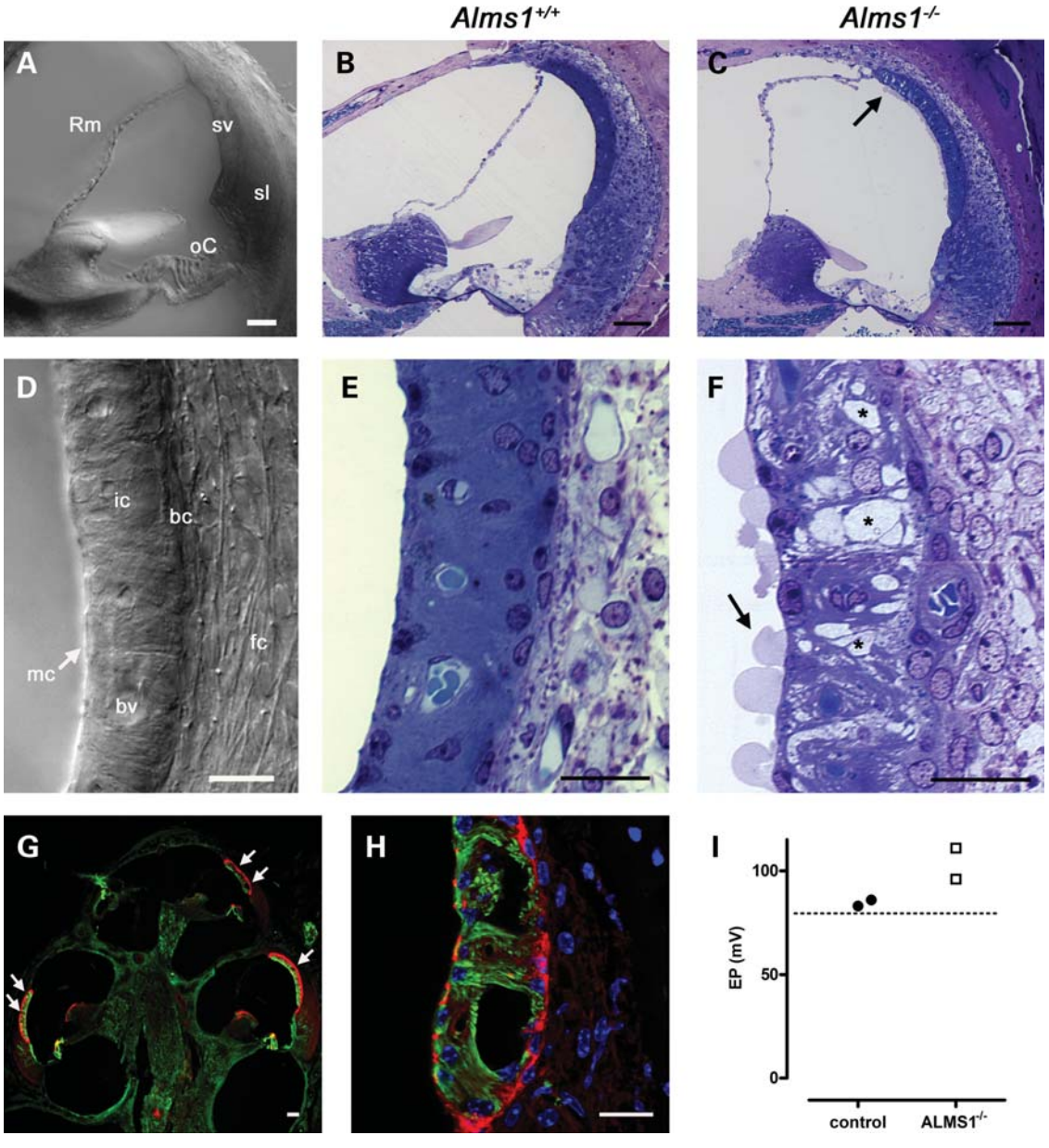

Figure 8. Ultra-structural changes in stria vascularis of *Alms1*$^{-/-}$ mice. (**A**–**D**) Photomicrographs of cochlear sections from P191 *Alms1*$^{+/+}$ and *Alms1*$^{-/-}$ mice. (A) DIC photomicrograph detailing the basal turn region of the cochlea (Rm, Reissner's membrane; oC, organ of Corti; sv, stria vascularis, sv; sl, spiral ligament). (B) The basal turn region of *Alms1*$^{+/+}$ cochlea. (C) The basal turn region of *Alms1*$^{-/-}$ cochlea. There were defects in the ultra-structure of the upper area of stria vascularis (arrow). (D) DIC photomicrograph detailing the tissues of the cochlear lateral wall (mc, marginal cell layer; ic, intermediate cell layer; bv, blood vessel; bc, basal cell layer; fc, spiral ligament fibrocytes). (**E**) Detail of the stria vascularis of *Alms1*$^{+/+}$ mouse, showing homogenous structure with basal cell, intermediate cell and marginal cell layers all present. (**F**) Detail of the stria vascularis of *Alms1*$^{-/-}$ mouse, showing large spaces within the intermediate cell layer (denoted *). There were large blebs on the apical (lumenal) membranes of marginal cells (arrow). (**G** and **H**) Projections of confocal image stacks of cochlear cryo-sections from an *Alms1*$^{-/-}$ mouse, labeled with an antibody against acetylated tubulin (green) that labels cytoplasmic microtubules in marginal cells, and phalloidin (red) that labels the basal cell layer and the apical region of marginal cells. (G) Large intercellular spaces in stria vascularis (arrows) were apparent in all cochlear turns. (H) Detail of very large lesions in the lower region of stria vascularis in the apical turn region. (**I**) Endocochlear potential (EP) values for individual control mice and *Alms1*$^{-/-}$ mice were within the normal range. Dashed line shows the +80 mV level for reference. Scale bars 20 μm.

cell loss was a direct consequence of the bundle abnormalities observed earlier in development, as these peculiarities were equally distributed along the cochlear partition. What seems more likely, also considering the parallel progressive atrophy of stria vascularis, is that as a consequence of the disruption of *Alms1*, these animals suffer from a more general deficit in tissue homeostasis.

Role of ALMS1 in cochlear development and hearing function

ALMS1 was immunolocalized specifically to the ciliary basal bodies of neonatal cochlear cells. This suggests that ALMS1 contributes to ciliary function in the cochlea. A comparable developmental expression pattern has been reported for

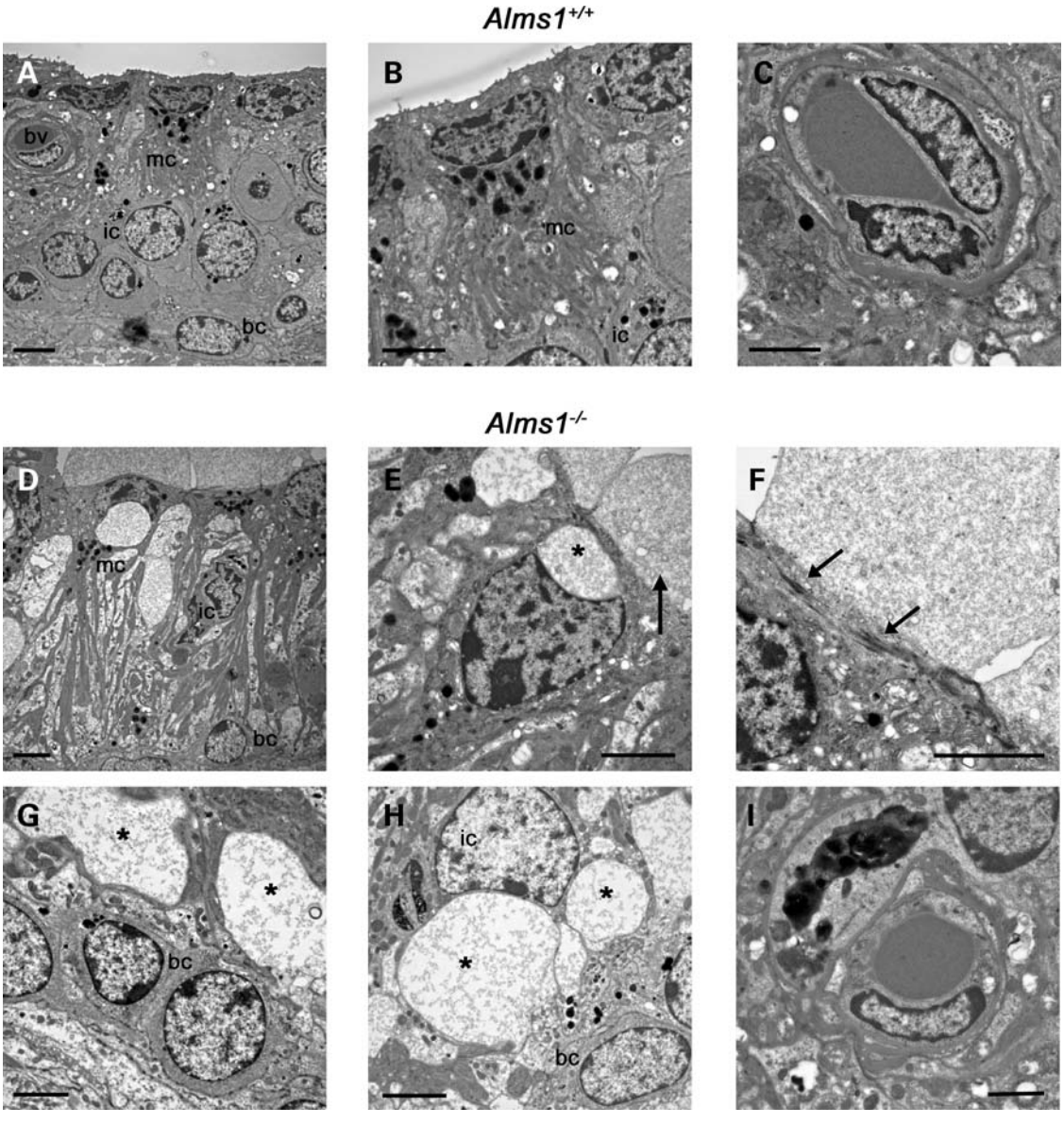

Figure 9. Formation of membrane-bound intracellular vacuoles in *Alms1*$^{-/-}$ mice. (**A**–**I**) Transmission electron micrographs of stria vascularis from P191 *Alms1*$^{+/+}$ and *Alms1*$^{-/-}$ mice. (A) Normal appearance of *Alms1*$^{+/+}$ mouse stria vascularis, including marginal cells (mc), intermediate cells (ic), basal cells (bc) and a blood vessel (bv). (B) Detail of a single marginal cell. (C) Detail of a blood vessel. (D) Abnormal appearance of *Alms1*$^{-/-}$ mouse stria vascularis. Large spaces were apparent in the intermediate cell layer, and nuclei in marginal cells and basal cells were atypical in shape. (E) Detail of a single marginal cell, showing a sub-cellular vacuole (marked *) above the nucleus and a bleb extending from the apical membrane (arrow). (F) Detail of the apical membrane of a marginal cell, showing amorphous material in the apical bleb, and microfilament assemblies bordering the bleb (arrows). (G) Large membrane-bound intracellular vacuoles (*) in the intermediate cell layer, above the basal cell layer. The vacuoles contained cytoplasmic material. (H) Large membrane-bound intracellular vacuoles (*) inside an intermediate cell causing deformation of the nucleus. (I) Normal appearance of a blood vessel. Scale bars, 2 μm.

BBS6/MKKS (13), a protein associated with BBS. There is a sub-clinical hearing loss in BBS patients and significant hearing loss in mouse models of the disease (23). In the mature cochlea, BBS6/MKKS was immunolocalized to non-centrosomal regions of hair cells and spiral ganglion neurons, suggesting a diversity of roles for this protein. Similarly, BBS2 and BBS4 were localized to non-centrosomal regions of cochlear cells and showed age-dependent associations with the actin and tubulin elements of the cytoskeleton. Non-centrosomal associations were not observed for ALMS1 at any developmental age studied here, suggesting this protein does not play diverse BBS-like non-centrosomal roles during development of the cochlea. The outer hair cell stereociliary bundle abnormalities seen in *Alms1*$^{-/-}$ mice are reminiscent of those observed in mouse models of BBS (13,23). This suggests that ALMS1 and certain BBS proteins may share common roles during development and contribute to common ciliary signaling pathways. Ciliogenesis appears normal in *Alms1*$^{-/-}$ mice, but aberrant positioning of the kinocilium seems to be a key factor in the abnormalities of bundle formation. This suggests that ALMS1 plays a role in the basal body migration and/or anchoring that determines

the final planar polarization of the cell. The occurrence of bundle abnormalities was comparable in P2 and P22 outer hair cells. This suggests that ALMS1 is important in the early determination of bundle polarity, a programming that is carried into maturity.

The developmental effects of *Alms1* disruption were immediately evident in the cochleae of every *Alms1*$^{-/-}$ mouse analyzed, but they were never observed in control animals. The number of outer hair cell bundles affected by the mutation appeared to be quite low (17–23% in all tonotopic locations). However, the occurrence of bundle abnormalities was comparable with that in *Bbs* mutant mice (23). This suggests that disruption of Alms1 renders the outer hair cell susceptible to a developmental abnormality that is perhaps triggered by stochastic developmental processes. Whereas the V-shape of the outer hair cell bundle appears to be dependent on ALMS1, the development of inner hair cell bundles did not appear to be affected in *Alms1*-disrupted mice. This suggests that the characteristic 'palisade' bundle formation of inner hair cells may not be dependent on the same polarity pathways controlling outer hair cell development. Inner hair cell bundles are not deformed in some other cilium-associated PCP mouse models (23,25).

The persistent expression of ALMS1 in mature tissues suggests that it also plays roles in a diverse range of physiological processes. ALMS1 was expressed in non-sensory supporting cells in the organ of Corti, epithelial cells which have recognized roles in cochlear homeostasis and are responsible for the longevity of hair cells (47). Within the mature cochlear lateral wall, ALMS1 was concentrated in centrioles of spiral ligament fibrocytes and of basal cells and intermediate cells in stria vascularis. It is possible that the progressive strial atrophy may result from deficiencies in the homeostatic function of these cells. The vacuoles in affected intermediate cells and marginal cells may result from pathological processes in ion transport. These effects deserve further study, in order to better describe the cellular basis of the human disease, not only in the ear but also in ion-transporting tissues affected in Alström Syndrome, such as the kidney. Renal disease in another mouse model of Alström Syndrome has been attributed to the progressive loss of cilium-dependent homeostasis and apoptosis (10). The progressive loss of hair cells from the organ of Corti and intermediate cells from stria vascularis further point towards alternative roles for ALMS1, beyond its hypothesized contribution to ciliary function. Cilia are reabsorbed into cells around the onset of hearing and so are unlikely to be involved in the mature function of these epithelial tissues. It is possible that the *Alms1*-associated pathology in the cochlea may be related to the life-threatening fibrosis seen in older Alström Syndrome patients (4,5,8). Organ fibrosis is an important phenotype in other ciliopathies (48), and the common pathology seems likely to be a consequence of defects in tissue differentiation and maintenance.

In summary, we have investigated the role of ALMS1 in the development of the cochlea, and the cellular basis of hearing loss in *Alms1*$^{-/-}$ mice. This model displays developmental abnormalities in stereociliary bundles consistent with ALMS1 playing a role in the regulation of PCP. In mature animals, there is an accelerated loss of outer hair cells from the sensory epithelium, and cell death within the ion transporting tissue stria vascularis. Further studies should determine how these abnormalities relate to the hearing loss and other tissue pathologies suffered by Alström Syndrome patients.

MATERIALS AND METHODS

Animals

Alms1 disrupted mice (B6; 129P2-*Alms1*$^{Gt(XH152)Byg}$/Pjn) were generated from gene-trapped ES cells (MMRRC# 008633) as described previously (30). To generate a fully congenic strain, F1 mice were successively backcrossed 10 generations to C57BL/6J. Mice homozygous for the targeted mutation, termed hereafter as *Alms1*$^{-/-}$, and control littermates were maintained in the Research Animal Facility at The Jackson Laboratory. Sprague–Dawley rats were raised and maintained at University College London. Rats were used primarily for immunolocalization experiments to avoid 'mouse-on-mouse' false positives in intact tissues that can occur when using antibodies raised in mice. All procedures were carried out under institutional ethics committee approval and federal guidelines.

Antibodies

ALMS1 was immunolocalized using a rabbit polyclonal antibody characterized elsewhere (9). This antibody was raised against the N-terminal amino acids (1–13) of human ALMS1, and in western blots of Jurkat whole-cell lysate it recognizes a band at the predicted molecular weight of ALMS1 at 461 kDa. This antibody was used at a final concentration of 1:100. In preliminary experiments, comparable results were seen in cochlear tissue and cells fixed with acetone/methanol/H_2O (9), or with 4% paraformaldehyde (PFA). Other primary antibodies were used at the following concentrations: mouse monoclonal anti-acetylated tubulin (1:1000; Sigma); mouse monoclonal anti-γ-tubulin (1:1000; Sigma); rabbit polyclonal anti-KIR4.1 (1:400; Alomone Labs); rabbit polyclonal anti-GLUT1 (1:400; Zymed); goat polyclonal anti-KCNQ1 (1:1000; Santa Cruz); and rabbit polyclonal anti-CX30 (1:400; Zymed).

Tissue preparation for immunofluorescence

The cochleae were isolated and fixed by direct perfusion with 4% PFA in phosphate-buffered saline (PBS) for 30 min at room temperature. They were then decalcified in 4% ethylene–diamine–tetraacetic acid (EDTA) in PBS, pH 7.3, for 24–48 h. For whole-mount preparations, the organs of Corti were dissected prior to staining. For transverse cryosections, entire decalcified cochleae were cryo-protected in 30% sucrose overnight, embedded low melting temperature agarose and snap frozen before sections were cut on a cryostat at 15 μm thickness. Sections were mounted on glass slides and dried at 45°C for 5 min before storage at −80°C. For vibratome sections, cochleae were decalcified in 4% EDTA overnight at 4°C and then mounted on a vibratome block and sectioned at 200 μm thickness, as described elsewhere (39).

Confocal immunofluorescence

Following fixation, tissues were permeabilized and blocked (0.1% Triton X-100 with 10% normal goat serum in PBS) for 30 min at room temperature, and then incubated in primary antibodies overnight at 4°C. Following several PBS washes, they were incubated in Alexa-Fluor tagged secondary antibodies (Invitrogen) in the dark for 30 min at room temperature. In some experiments, microtubules were stained with the mouse monoclonal anti-acetylated tubulin primary antibody. Actin was stained with tetramethyl-rhodamine phalloidin (Sigma) at 1:1000. Cells or tissues were mounted on glass slides using Vectashield with diamidino-2-phenylindole (DAPI, Vector Laboratories). Imaging was carried out using a laser scanning confocal microscope (LSM510; Carl Zeiss MicroImaging) as described elsewhere (39). Micrographs were converted to TIFF format and adjusted for optimal contrast and brightness using Adobe Photoshop software.

Light and electron microscopy

For differential interference contrast (DIC) microscopy, vibratome cochlear slices were prepared as above. Slices were mounted on glass slides in Vectashield, and images were taken on an upright microscope fitted with a digital camera controlled by Axiovision software (Carl Zeiss MicroImaging). For electron microscopy, tissues were fixed *in situ* by direct perfusion of the cochleae with 2.5% glutaraldehyde in 0.1 M cacodylate buffer for 2 h at room temperature, then post-fixed in OsO_4 for 2 h at room temperature. The cochleae were then decalcified in 4% EDTA in cacodylate buffer for 48 h. For sectioning, the entire decalcified cochleae were dehydrated in an alcohol series to 70% ethanol, exposed en bloc to a saturated solution of uranyl acetate in 70% ethanol overnight at 4°C, before completion of dehydration and embedding in plastic. Sections of the entire cochlea for light microscopy were cut at 1 μm thickness and stained with toluidine blue, before thin sections for TEM were obtained. All sections contained the entire height of the cochlea and sections were cut at several different depths through it to enable assessment of the entire cochlear spiral (37). For SEM, the organs of Corti were dissected from cochleae following fixation and decalcification as above. The dissected segments were then processed through the repeated thiocarbohydrazide-OsO_4 procedure (49), critical point dried and lightly sputter-coated with platinum before examination.

Tests of auditory physiology

In animals subsequently used for confocal and electron microscopy, ABRs were carried out as described previously (30). In a separate group of mice, ABRs, DPOAEs and EPs were all carried out under anesthetic (ketamine 65 mg/kg, xylazine 3.5 mg/kg and acepromazine 2 mg/kg), and body temperature maintained using water-circulation heat pads and lamps. ABRs were recorded in an electrically and acoustically shielded chamber (Acoustic Systems). Needle electrodes were placed at vertex (active) and the test ear (reference) and contra-lateral ear (ground) pinnae. Tucker Davis Technologies (TDT) System III hardware and SigGen/BioSig software (TDT) were used to present the stimulus and record responses. Tones were delivered through an EC1 driver (TDT, aluminum enclosure made in-house), with the speculum placed just inside the tragus. Stimulus presentation was 15 ms tone bursts, with 1 ms rise/fall times, presented 10 per s. Up to 1024 responses were averaged for each stimulus level. Responses were collected for stimulus levels in 10 dB steps at higher stimulus levels, with additional 5 dB steps near threshold. Thresholds were interpolated between the lowest stimulus level where a response was observed, and 5 dB lower, where no response was observed. For DPOAEs, the primary tones, F1 and F2, were set at a ratio of F2/F1 = 1.2. The intensity of F1 (L1) was varied in 5 or 10 dB steps, with the intensity of F2 (L2) held at 10 dB quieter than L1. The DPOAE was measured at 2F1 – F2. Tones are presented via two EC1 drivers (TDT) connected through an Etymotic microphone (ER 10B+, Etymotic Research, Inc.). TDT System III hardware and SigGen/BioSig software are used to present the stimuli and record responses. For EPs, mice were placed in a head-holder, the external pinna removed and soft tissue dissected away from the bulla. The ossicles and tympanic membrane were removed and some of the bulla wall was removed to allow clear visualization of the cochlea. A small opening was made in the otic capsule over the stria vascularis for penetration of a glass micropipette (filled with 150 mM KCl) into scala media. The micropipette was inserted with a hydraulic microdrive (1:1, 50 μm per revolution). The electrode signals were amplified by a capacity-compensated dc preamplifier and recorded using TDT hardware and 'chart recorder' software written in-house.

SUPPLEMENTARY MATERIAL

Supplementary Material is available at *HMG* online.

ACKNOWLEDGEMENTS

We thank Professor David Wilson (University of Southampton, UK) for the gift of the N-terminal ALMS1 antibody. BBS mutant mice were supplied by Professor Phil Beales (University College London, UK).

Conflict of Interest statement. None declared.

FUNDING

This work was funded by the Biotechnology and Biological Sciences Research Council (Grant BB/D009669/1 to D.J. and A.F.), Deafness Research UK (Grant 358.CAR.DJ to D.J.; Grant 294.ILO:AF to A.F.) and the National Institutes of Health (Grant HD036878 to J.N., G.C., J.M.; Grant DC04301 to C.L.-G.; P30 Grant DC05188 to D.D.). D.J. is a Royal Society University Research Fellow (Grant 516002.K5746.KK).

REFERENCES

1. Collin, G.B., Marshall, J.D., Ikeda, A., So, W.V., Russell-Eggitt, I., Maffei, P., Beck, S., Boerkoel, C.F., Sicolo, N., Martin, M. *et al.* (2002) Mutations in ALMS1 cause obesity, type 2 diabetes and neurosensory degeneration in Alstrom syndrome. *Nat. Genet.*, **31**, 74–78.

2. Hearn, T., Renforth, G.L., Spalluto, C., Hanley, N.A., Piper, K., Brickwood, S., White, C., Connolly, V., Taylor, J.F., Russell-Eggitt, I. *et al.* (2002) Mutation of ALMS1, a large gene with a tandem repeat encoding 47 amino acids, causes Alstrom syndrome. *Nat. Genet.*, **31**, 79–83.
3. Alström, C.H., Hallgren, B., Nilsson, L.B. and Asander, H. (1959) Retinal degeneration combined with obesity, diabetes mellitus and neurogenous deafness: a specific syndrome (not hitherto described) distinct from the Laurence–Moon–Bardet–Biedl syndrome: a clinical, endocrinological and genetic examination based on a large pedigree. *Acta Psychiatr. Neurol. Scand. Suppl.*, **129**, 1–35.
4. Marshall, J.D., Bronson, R.T., Collin, G.B., Nordstrom, A.D., Maffei, P., Paisey, R.B., Carey, C., Macdermott, S., Russell-Eggitt, I., Shea, S.E. *et al.* (2005) New Alstrom syndrome phenotypes based on the evaluation of 182 cases. *Arch. Intern. Med.*, **165**, 675–683.
5. Marshall, J.D., Beck, S., Maffei, P. and Naggert, J.K. (2007) Alstrom syndrome. *Eur. J. Hum. Genet.*, **15**, 1193–1202.
6. Marshall, J.D., Hinman, E.G., Collin, G.B., Beck, S., Cerqueira, R., Maffei, P., Milan, G., Zhang, W., Wilson, D.I., Hearn, T. *et al.* (2007) Spectrum of ALMS1 variants and evaluation of genotype–phenotype correlations in Alstrom syndrome. *Hum. Mutat.*, **28**, 1114–1123.
7. Welsh, L.W. (2007) Alstrom syndrome: progressive deafness and blindness. *Ann. Otol. Rhinol. Laryngol.*, **116**, 281–285.
8. Loudon, M.A., Bellenger, N.G., Carey, C.M. and Paisey, R.B. (2009) Cardiac magnetic resonance imaging in Alstrom syndrome. *Orphanet. J. Rare Dis.*, **4**, 14.
9. Hearn, T., Spalluto, C., Phillips, V.J., Renforth, G.L., Copin, N., Hanley, N.A. and Wilson, D.I. (2005) Subcellular localization of ALMS1 supports involvement of centrosome and basal body dysfunction in the pathogenesis of obesity, insulin resistance, and type 2 diabetes. *Diabetes*, **54**, 1581–1587.
10. Li, G., Vega, R., Nelms, K., Gekakis, N., Goodnow, C., McNamara, P., Wu, H., Hong, N.A. and Glynne, R. (2007) A role for Alstrom syndrome protein, alms1, in kidney ciliogenesis and cellular quiescence. *PLoS Genet.*, **3**, e8.
11. Knorz, V.J., Spalluto, C., Lessard, M., Purvis, T.L., Adigun, F.F., Collin, G.B., Hanley, N.A., Wilson, D.I. and Hearn, T. (2010) Centriolar association of ALMS1 and likely centrosomal functions of the ALMS motif-containing proteins C10orf90 and KIAA1731. *Mol. Biol. Cell.*, **21**, 3617–3629.
12. Nachury, M.V., Loktev, A.V., Zhang, Q., Westlake, C.J., Peranen, J., Merdes, A., Slusarski, D.C., Scheller, R.H., Bazan, J.F., Sheffield, V.C. *et al.* (2007) A core complex of BBS proteins cooperates with the GTPase Rab8 to promote ciliary membrane biogenesis. *Cell*, **129**, 1201–1213.
13. May-Simera, H.L., Ross, A., Rix, S., Forge, A., Beales, P.L. and Jagger, D.J. (2009) Patterns of expression of Bardet–Biedl syndrome proteins in the mammalian cochlea suggest noncentrosomal functions. *J. Comp. Neurol.*, **514**, 174–188.
14. Ansley, S.J., Badano, J.L., Blacque, O.E., Hill, J., Hoskins, B.E., Leitch, C.C., Kim, J.C., Ross, A.J., Eichers, E.R., Teslovich, T.M. *et al.* (2003) Basal body dysfunction is a likely cause of pleiotropic Bardet–Biedl syndrome. *Nature*, **425**, 628–633.
15. Kim, J.C., Ou, Y.Y., Badano, J.L., Esmail, M.A., Leitch, C.C., Fiedrich, E., Beales, P.L., Archibald, J.M., Katsanis, N., Rattner, J.B. *et al.* (2005) MKKS/BBS6, a divergent chaperonin-like protein linked to the obesity disorder Bardet–Biedl syndrome, is a novel centrosomal component required for cytokinesis. *J. Cell Sci.*, **118**, 1007–1020.
16. Kim, J.C., Badano, J.L., Sibold, S., Esmail, M.A., Hill, J., Hoskins, B.E., Leitch, C.C., Venner, K., Ansley, S.J., Ross, A.J. *et al.* (2004) The Bardet–Biedl protein BBS4 targets cargo to the pericentriolar region and is required for microtubule anchoring and cell cycle progression. *Nat. Genet.*, **36**, 462–470.
17. Yen, H.J., Tayeh, M.K., Mullins, R.F., Stone, E.M., Sheffield, V.C. and Slusarski, D.C. (2006) Bardet–Biedl syndrome genes are important in retrograde intracellular trafficking and Kupffer's vesicle cilia function. *Hum. Mol. Genet.*, **15**, 667–677.
18. Kim, S.K., Shindo, A., Park, T.J., Oh, E.C., Ghosh, S., Gray, R.S., Lewis, R.A., Johnson, C.A., Attie-Bittach, T., Katsanis, N. *et al.* (2010) Planar cell polarity acts through septins to control collective cell movement and ciliogenesis. *Science*, **329**, 1337–1440.
19. Wiens, C.J., Tong, Y., Esmail, M.A., Oh, E., Gerdes, J.M., Wang, J., Tempel, W., Rattner, J.B., Katsanis, N., Park, H.W. *et al.* (2010) Bardet-Biedl syndrome-associated small GTPase ARL6 (BBS3) functions at or near the ciliary gate and modulates Wnt signaling. *J. Biol. Chem.*, **285**, 16218–16230.
20. Badano, J.L., Mitsuma, N., Beales, P.L. and Katsanis, N. (2006) The ciliopathies: an emerging class of human genetic disorders. *Annu. Rev. Genomics Hum. Genet.*, **7**, 125–148.
21. Fliegauf, M., Benzing, T. and Omran, H. (2007) When cilia go bad: cilia defects and ciliopathies. *Nat. Rev. Mol. Cell Biol.*, **8**, 880–893.
22. Adams, M., Smith, U.M., Logan, C.V. and Johnson, C.A. (2008) Recent advances in the molecular pathology, cell biology and genetics of ciliopathies. *J. Med. Genet.*, **45**, 257–267.
23. Ross, A.J., May-Simera, H., Eichers, E.R., Kai, M., Hill, J., Jagger, D.J., Leitch, C.C., Chapple, J.P., Munro, P.M., Fisher, S. *et al.* (2005) Disruption of Bardet–Biedl syndrome ciliary proteins perturbs planar cell polarity in vertebrates. *Nat. Genet.*, **37**, 1135–1140.
24. Dabdoub, A. and Kelley, M.W. (2005) Planar cell polarity and a potential role for a Wnt morphogen gradient in stereociliary bundle orientation in the mammalian inner ear. *J. Neurobiol.*, **64**, 446–457.
25. Jones, C., Roper, V.C., Foucher, I., Qian, D., Banizs, B., Petit, C., Yoder, B.K. and Chen, P. (2008) Ciliary proteins link basal body polarization to planar cell polarity regulation. *Nat. Genet.*, **40**, 69–77.
26. Jones, C. and Chen, P. (2008) Primary cilia in planar cell polarity regulation of the inner ear. *Curr. Top. Dev. Biol.*, **85**, 197–224.
27. Denman-Johnson, K. and Forge, A. (1999) Establishment of hair bundle polarity and orientation in the developing vestibular system of the mouse. *J. Neurocytol.*, **28**, 821–835.
28. Lagziel, A., Ahmed, Z.M., Schultz, J.M., Morell, R.J., Belyantseva, I.A. and Friedman, T.B. (2005) Spatiotemporal pattern and isoforms of cadherin 23 in wild type and waltzer mice during inner ear hair cell development. *Dev. Biol.*, **280**, 295–306.
29. Brown, S.D., Hardisty-Hughes, R.E. and Mburu, P. (2008) Quiet as a mouse: dissecting the molecular and genetic basis of hearing. *Nat. Rev. Genet.*, **9**, 277–290.
30. Collin, G.B., Cyr, E., Bronson, R., Marshall, J.D., Gifford, E.J., Hicks, W., Murray, S.A., Zheng, Q.Y., Smith, R.S., Nishina, P.M. *et al.* (2005) Alms1-disrupted mice recapitulate human Alstrom syndrome. *Hum. Mol. Genet.*, **14**, 2323–2333.
31. Trowe, M.O., Maier, H., Schweizer, M. and Kispert, A. (2008) Deafness in mice lacking the T-box transcription factor Tbx18 in otic fibrocytes. *Development*, **135**, 1725–1734.
32. Wangemann, P. (2002) K+ cycling and the endocochlear potential. *Hear. Res.*, **165**, 1–9.
33. Leibovici, M., Verpy, E., Goodyear, R.J., Zwaenepoel, I., Blanchard, S., Laine, S., Richardson, G.P. and Petit, C. (2005) Initial characterization of kinocilin, a protein of the hair cell kinocilium. *Hear. Res.*, **203**, 144–153.
34. Nakazawa, K., Spicer, S.S., Gratton, M.A. and Schulte, B.A. (1996) Localization of actin in basal cells of stria vascularis. *Hear. Res.*, **96**, 13–19.
35. Karolyi, I.J., Dootz, G.A., Halsey, K., Beyer, L., Probst, F.J., Johnson, K.R., Parlow, A.F., Raphael, Y., Dolan, D.F. and Camper, S.A. (2007) Dietary thyroid hormone replacement ameliorates hearing deficits in hypothyroid mice. *Mamm. Genome*, **18**, 596–608.
36. Noben-Trauth, K. and Johnson, K.R. (2009) Inheritance patterns of progressive hearing loss in laboratory strains of mice. *Brain Res.*, **1277**, 42–51.
37. Taylor, R.R., Nevill, G. and Forge, A. (2008) Rapid hair cell loss: a mouse model for cochlear lesions. *J. Assoc. Res. Otolaryngol.*, **9**, 44–64.
38. Ando, M. and Takeuchi, S. (1999) Immunological identification of an inward rectifier K+ channel (Kir4.1) in the intermediate cell (melanocyte) of the cochlear stria vascularis of gerbils and rats. *Cell Tissue Res.*, **298**, 179–183.
39. Jagger, D.J. and Forge, A. (2006) Compartmentalized and signal-selective gap junctional coupling in the hearing cochlea. *J. Neurosci.*, **26**, 1260–1268.
40. Demeester, K., van Wieringen, A., Hendrickx, J.J., Topsakal, V., Fransen, E., van Laer, L., Van Camp, G. and Van de Heyning, P. (2009) Audiometric shape and presbycusis. *Int. J. Audiol.*, **48**, 222–232.
41. Schmiedt, R.A., Lang, H., Okamura, H.O. and Schulte, B.A. (2002) Effects of furosemide applied chronically to the round window: a model of metabolic presbyacusis. *J. Neurosci.*, **22**, 9643–9650.
42. Schuknecht, H.F. and Gacek, M.R. (1993) Cochlear pathology in presbycusis. *Ann. Otol. Rhinol. Laryngol.*, **102**, 1–16.

43. Schulte, B.A. and Schmiedt, R.A. (1992) Lateral wall Na,K-ATPase and endocochlear potentials decline with age in quiet-reared gerbils. *Hear. Res.*, **61**, 35–46.
44. Wangemann, P., Itza, E.M., Albrecht, B., Wu, T., Jabba, S.V., Maganti, R.J., Lee, J.H., Everett, L.A., Wall, S.M., Royaux, I.E. *et al.* (2004) Loss of KCNJ10 protein expression abolishes endocochlear potential and causes deafness in Pendred syndrome mouse model. *BMC Med.*, **2**, 30.
45. Mustapha, M., Fang, Q., Gong, T.W., Dolan, D.F., Raphael, Y., Camper, S.A. and Duncan, R.K. (2009) Deafness and permanently reduced potassium channel gene expression and function in hypothyroid Pit1dw mutants. *J. Neurosci.*, **29**, 1212–1223.
46. Hirose, K. and Liberman, M.C. (2003) Lateral wall histopathology and endocochlear potential in the noise-damaged mouse cochlea. *J. Assoc. Res. Otolaryngol.*, **4**, 339–352.
47. Gale, J.E. and Jagger, D.J. (2010) Cochlear supporting cells. In Fuchs, P.A. (ed.), *The Oxford Handbook of Auditory Science: The Ear*. Oxford University Press, Oxford, UK, pp. 307–327.
48. Hildebrandt, F. and Zhou, W. (2007) Nephronophthisis-associated ciliopathies. *J. Am. Soc. Nephrol.*, **18**, 1855–1871.
49. Davies, S. and Forge, A. (1987) Preparation of the mammalian organ of Corti for scanning electron microscopy. *J. Microsc.*, **147**, 89–101.